Scripta Materialia 241 (2024) 115886

Contents lists available at ScienceDirect

Scripta Materialia

journal homepage: www.journals.elsevier.com/scripta-materialia

Al-Mn-based decagonal quasicrystal in AZ magnesium alloys and its nucleation on Al_8Mn_5 during solidification

Di Wang [a], Liuqing Peng [a,b,*], Christopher M. Gourlay [a,*]

[a] Department of Materials, Imperial College London, London SW7 2AZ, UK

[b] National Engineering Research Centre for Magnesium Alloy, Chongqing University, Chongqing 400044, China

ARTICLE INFO

Keywords:
Quasicrystal
Analytical electron microscopy
Intermetallic compounds
Heterogeneous nucleation of phase transformation
Multicomponent solidification

ABSTRACT

Manganese is added to many magnesium alloys to control impurity iron, but its effects on phase transformations and microstructure formation remain incompletely understood. Here we show that an Al-Mn-based decagonal quasicrystal (d-QC) forms in the late stages of solidification in AZ31 and AZ91 magnesium alloys at relatively slow cooling rates, here down to 0.1 K/s. The d-QC has a periodicity of ~ 12 Å, grew as decagonal rods and commonly shared interfaces with Al_8Mn_5 and eutectic $Mg_{17}Al_{12}$. A reproducible orientation relationship (OR) was measured with Al_8Mn_5 only, indicating that the d-QC nucleated on Al_8Mn_5. The OR is consistent with the structural relationship between quasicrystals and gamma brasses and gives the d-QC nucleation advantages over LT-$Al_{11}Mn_4$ during solidification. A subsequent heat treatment at 410 °C caused both Al_8Mn_5 and the d-QC to transform into LT-$Al_{11}Mn_4$.

Many magnesium alloys, including the AM- and AZ- series, contain aluminium and a small (0.1 – 0.5 wt%) manganese addition [1]. The latter reduces the impurity iron content in the melt prior to casting [2] and ensures the iron remaining in the liquid crystallises into Al-(Mn,Fe) intermetallic compounds (IMCs) instead of Al-Fe IMCs which prevents excessive micro-galvanic corrosion of the α-Mg phase [3]. However, the Mn addition also adds significant complexity to the solidification sequence and results in multiple Al-Mn IMCs whose formation remains incompletely understood. For example, consider the Mg-rich corner of the Mg-Al-Mn liquidus projection in Fig. 1(a). The Scheil solidification paths are superimposed for Mg-3Al-0.5Mn, Mg-9Al-0.2Mn and Mg-9Al-0.06Mn (wt.%). The first two have Al_8Mn_5 as the primary phase while the latter has α-Mg as the primary phase. Then, in all three alloys, the liquid composition follows the same eutectic grooves and passes two quasi-peritectic points involving α-Mg and various Al-Mn IMCs (Al_8Mn_5, LT-$Al_{11}Mn_4$ and then μ-Al_4Mn) until it reaches the ternary eutectic point of α-Mg+$Mg_{17}Al_{12}$+μ-Al_4Mn. The results in Fig. 1(a) are only subtly different for alloys with a dilute Zn addition such as AZ31 and AZ91 since Zn has negligible solubility in these Al-Mn intermetallics [4].

Past experimental work on cast AZ31 and AZ91 has presented clear evidence (with diffraction) for $Mg_{17}Al_{12}$ [5],[6], Al_8Mn_5 [7] [8,9,10,11,12], and LT-$Al_{11}Mn_4$ [10],[11], after solidification but μ-Al_4Mn has not been identified conclusively in these alloys. Additionally, LT-$Al_{11}Mn_4$ is usually only present in trace amounts after solidification unless very low cooling rates are applied (0.1 K s^{-1} in [10]). This indicates that the Al-Mn intermetallics formed in the last stages of AZ31 and AZ91 solidification may exhibit nucleation and growth difficulties and metastability. Therefore, there is a need for a study to better understand Al-Mn phase formation in the last stages of solidification in AZ31 and AZ91.

Al-Mn intermetallics have been studied intensively in binary Al-Mn alloys and Al-Mn-TM alloys (TM = another transition metal) [13,14,15,16], and icosahedral quasicrystals (i-QCs) [17] and decagonal quasicrystals (d-QCs) [18,19], were first discovered in this system. In the latter stages of Mg-(3–9)Al-xMn alloy solidification (Fig. 1(a)) the calculated equilibrium Al-Mn compounds (LT-$Al_{11}Mn_4$ and then μ-Al_4Mn [4]) have compositions in the range 73 – 80 at.% Al which is similar to multiple known equilibrium and metastable Al-Mn phases including an i-QC and d-QC [17,18,20,21,22,23,13,24]. However, an interesting difference is that the 'low temperature' Al_8Mn_5 and LT-$Al_{11}Mn_4$ phases crystallise in magnesium-rich liquid in Mg-Al-Mn-based alloys [25] whereas they do not exist in equilibrium with liquid in the binary Al-Mn system [13,26,27]. This makes magnesium-aluminium-manganese alloy solidification an interesting space to gain new insights into the competition and cooperation

* Corresponding authors.
E-mail addresses: liuqing.peng@cqu.edu.cn (L. Peng), c.gourlay@imperial.ac.uk (C.M. Gourlay).

https://doi.org/10.1016/j.scriptamat.2023.115886
Received 10 September 2023; Received in revised form 3 November 2023; Accepted 13 November 2023
1359-6462/

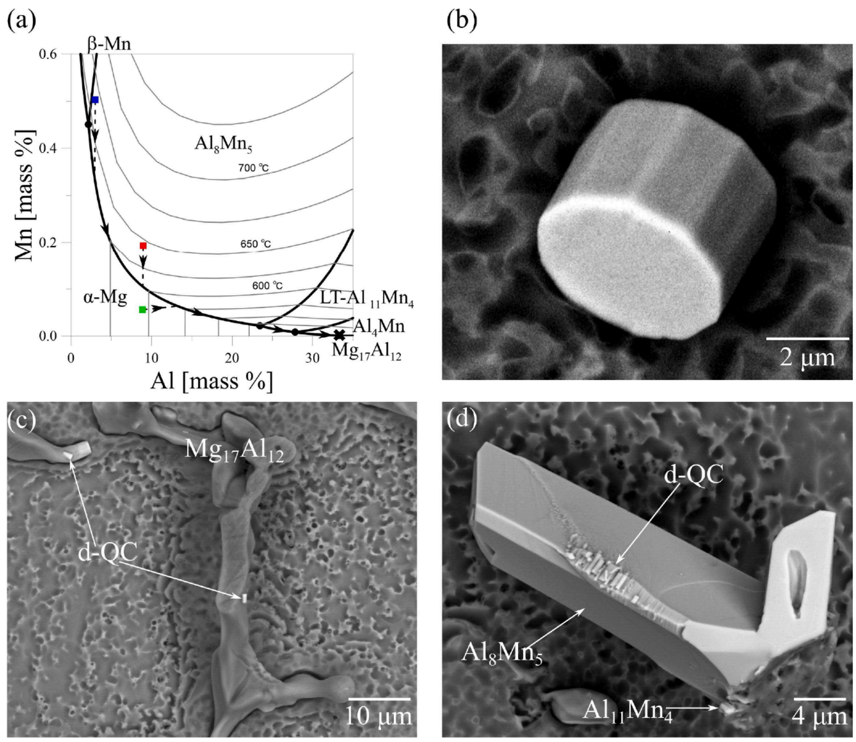

Fig. 1. (a) Calculated liquidus projection of the Mg-rich corner of the Mg-Al-Mn system from ThermoCalc database TCMG4. Scheil solidification paths of Mg-3Al-0.5Mn (blue), Mg-9Al-0.2Mn (red), and Mg-9Al-0.06Mn (green) are superimposed. *X*=the ternary eutectic point. (b)-(d) intermetallics in deep-etched Mg-9Al-0.7Zn-0.2Mn. (b) d-QC rod; (c) d-QC rods on $Mg_{17}Al_{12}$ and (d) d-QC rods on Al_8Mn_5.

Table 1
Compositions (wt%) of AZ31–0.5Mn, AZ91–0.06Mn and AZ91–0.2Mn.

	Mg	Al	Zn	Mn	Fe	Cu	Si	Ni
AZ31–0.5Mn	Bal.	3.09	1.06	0.49	0.003	0.002	0.067	<0.001
AZ91–0.06Mn	Bal.	9.24	0.76	0.056	0.0013	0.0008	0.035	0.0002
AZ91–0.2Mn	Bal.	8.95	0.72	0.19	<0.001	0.001	0.039	<0.001

amongst complex Al-Mn IMCs.

For this paper, we studied one AZ31 and two AZ91 alloys with compositions in Table 1, which are similar to the three alloys in Fig. 1(a). Three solidification conditions were applied: (i) gravity casting, (ii) melting ~2 g samples within Al_2O_3 cups in quartz tubes under Ar before placing the tube into a cylindrical hole in a room-temperature steel mould to solidify, and (iii) the same as (ii) but with furnace cooling. Detailed conditions for method (i) are given in ref. [28] and for methods (ii) and (iii) in ref. [10]. The cooling rates in the liquid prior to α-Mg nucleation were measured to be ~90 K s^{-1}, 4 K s^{-1} and 0.1 K s^{-1} by a K-type thermocouple, either within the cavity of the gravity casting mould or on the outside of the quartz tube. For the slowest cooling rate (method (iii)), samples were switched to cooling method (ii) from 410 °C to minimise any solid-state transformations.

Samples of each alloy were examined in the as-cast condition and the two AZ91 alloys were additionally examined after solution heat treatment in quartz tubes under Ar at 410 °C for 1 day and 15 days followed by quenching in water. For microstructural characterisation, some samples were prepared as polished cross-sections and others were deep etched using 10 % nitric acid in ethanol for 5–10 min to enable imaging of the 3D morphology of IMCs.

A ThermoFisher Scientific Helios 5CX dual-beam scanning electron microscope and focused ion beam (SEM-FIB) instrument was used for site-specific lift out of thin lamellae. These were then investigated by transmission electron microscopy (TEM) in a JEOL 2100F field-emission-gun (FEG) TEM. SEM imaging and electron back-scattered diffraction (EBSD) were conducted using two Zeiss Sigma-300 FEG-SEMs, one with a Bruker e^{-}FlashHR detector and the other with an EDAX Clarity detector.

In the three alloys and under all cooling conditions, it was found that an Al-Mn IMC was present with the morphology of decagonal rods as summarised in Fig. 1(b)-(d). Commonly, the rods shared interfaces with $Mg_{17}Al_{12}$ and Al_8Mn_5 as shown in the examples in Fig. 1(c)-(d). Structural characterisation of the Al-Mn rod phase by TEM selected area electron diffraction (SAED) confirmed that it is a decagonal quasicrystal (d-QC). Diffraction patterns of d-QC rods are shown in Fig. 2. FIB lamellae prepared such that the long rod axis was in the TEM incident beam direction gave SAED patterns along the 10-fold (d-10) axis, Fig. 2 (a)-(b), in which the directions of the two distinct 2-fold axes are labelled as 2D and 2P [29]. Both Fig. 2(a) and 2(b) show 10-fold rotational symmetry. Note that the SAED patterns in Fig. 2(a) and 2(b) were taken along the same orientation but at different camera length. Fig. 2(c) is the convergent beam electron diffraction (CBED) pattern from the same orientation as the SAED patterns, exhibiting 10-fold symmetry. Each Kikuchi band in Fig. 2(c) consists of two colinear bands with band width ratio=1.62 ~ τ (the golden mean ratio), arising from its quasi-periodic nature consistent with [30]. SAED patterns along the 2D and 2P directions are shown in Fig. 2(d) and Fig. 2(e) respectively, which were FIB milled to be 90° away from the rod axis (i.e. the 10-fold axis) and were 18° away from each other. SAED patterns along the 2D and 2P directions are periodic along the d-10 axis with a periodicity of ~12.3 Å, similar to the ~12 Å periodicity of the Al-Mn-type d-QC found

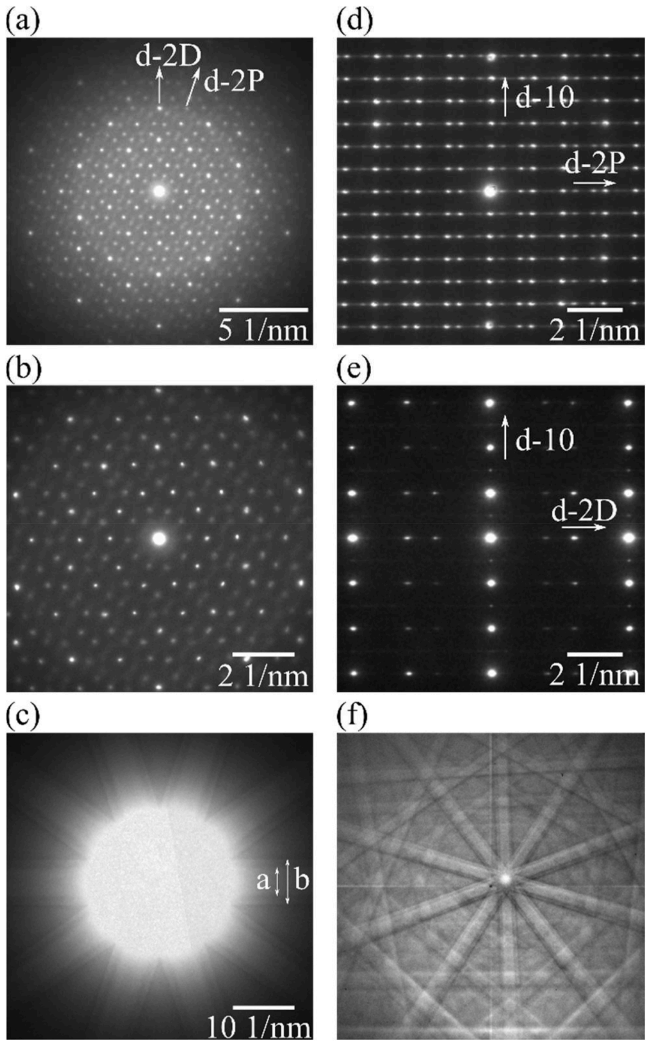

Fig. 2. Diffraction of the decagonal quasicrystal from AZ91–0.06Mn. (a)-(c): SAED and CBED taken along the longitudinal direction of a rod such as Fig. 1 (b). (b) is zoomed in of (a). All three show clear 10-fold symmetry. In (c) the ratio of band widths $b/a = 1.62 \sim \tau$. (d) and (e): SAED from 2D and 2P respectively, 18° a part to each other. (f): EBSD pattern with 10-fold axis near the centre.

Table 2
Composition (at.%) of d-QC, LT-$Al_{11}Mn_4$ and Al_8Mn_5 measured from TEM-EDS. [1]=AZ91–0.06Mn, [2]=AZ91–0.2Mn, [3]=AZ31–0.5Mn.

	Al	Mn	Mg	Fe
d-QC[1]	76.2	19.1	4.4	0.3
d-QC[2]	77.8	20.1	2.0	0.1
d-QC[3]	74.6	21.5	3.8	0.1
LT-$Al_{11}Mn_4$	76.0	23.5	0.5	–
Al_8Mn_5	61.2	38.6	0.3	–

by Bendersky [18]. This ~12 Å periodicity can also be expressed as a D_3 structure based on the D_i designation from [31]. An EBSD pattern from the d-QC with the 10-fold axis near the centre is shown in Fig. 2(f).

The chemical compositions of the Al-Mn IMCs measured from TEM energy dispersive X-ray spectroscopy (EDS) are shown in Table 2. The Al/Mn ratio of the d-QC is close to Al_4Mn, which is similar to prior studies on decagonal and approximant phases in Al-Mn alloys [18,32,33,34]. In addition, around 3 at.% Mg and 0.15 at.% Fe were found in the d-QC in this work. The d-QC in AZ31–0.5Mn has slightly less Al and more Mn than the d-QC in AZ91.

Table 3
Summary of Al-Mn IMCs in three AZ magnesium alloys with three different solidification conditions. $Al_{11}Mn_4$ refers to LT-$Al_{11}Mn_4$ [35].

Alloy Wt.%	Gravity casting ~90 K s^{-1}	Moderate cooling 4 K s^{-1}	Slow cooling 0.1 K s^{-1}
Mg-3Al-1.0Zn-0.5Mn	Al_8Mn_5 + d-QC	Al_8Mn_5 + $Al_{11}Mn_4$ + d-QC	Al_8Mn_5 + $Al_{11}Mn_4$ + d-QC
Mg-9Al-0.7Zn-0.2Mn	Al_8Mn_5 + d-QC	Al_8Mn_5 + $Al_{11}Mn_4$ + d-QC	Al_8Mn_5 + $Al_{11}Mn_4$ + d-QC
Mg-9Al-0.7Zn-0.06Mn	Al_8Mn_5 + d-QC	Al_8Mn_5 + $Al_{11}Mn_4$ + d-QC	–

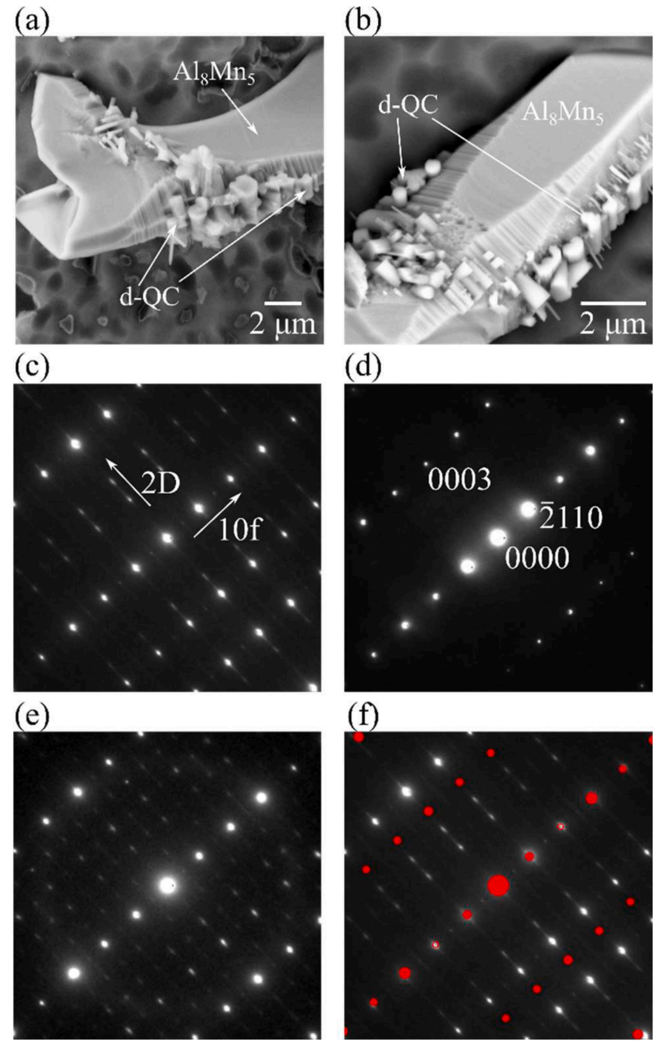

Fig. 3. Orientation relationship between Al_8Mn_5 and d-QC. (a)-(b) Al_8Mn_5 rods with d-QC on the surface from AZ91 with 0.2Mn sample. (c) SAED of d-QC along d-2P axis; (d) SAED of Al_8Mn_5 along $[01\bar{1}0]$; (e) SAED of both and (f) SAED of d-QC superimposed with simulated pattern of Al_8Mn_5. Two red circles are drawn in (f) to indicate the positions of simulated weak $(4\bar{2}\bar{2}0)$ and $(\bar{4}220)$ spots of Al_8Mn_5.

The Al-Mn IMCs found for each combination of composition and solidification condition are listed in Table 3. Al_8Mn_5, LT-$Al_{11}Mn_4$ and d-QC were all present at the lowest cooling rate (0.1 K s^{-1}). With increasing cooling rate, the fraction of d-QC increased and the fraction of LT-$Al_{11}Mn_4$ deceased until, in gravity castings, no LT-$Al_{11}Mn_4$ was found. No μ-Al_4Mn was detected in this work. The fraction of d-QC also increased with increasing Al/Mn ratio in the alloy; the highest fraction

Table 4
Approximant phases used for (mis)indexing EBSD patterns from the d-QC. Cross-correlation coefficients (CCC) quantify the match between one d-QC pattern and the best-matching simulated pattern for each approximant. Al_8Mn_5 and LT-$Al_{11}Mn_4$ are included to show their lattice parameters and EBSD pattern similarity to that of d-QC.

Phase	Space group	Pearson symbol	Lattice parameter (nm and°)						CCC	Ref.
			a	b	c	α	β	γ		
T-Al_3Mn	Pnma	*oP*156	1.48	1.24	1.26	90	90	90	0.478	[48]
R-Al_4Mn	Cmcm	*oS*156	2.36	1.24	0.77	90	90	90	0.427	[49]
Al_3Pd	$Pna2_1$	–	2.34	1.67	1.23	90	90	90	0.380	[50]
μ-Al_4Mn	$P6_3/mmc$	*hP*563	2.00	2.00	2.47	90	90	120	0.376	[20]
λ-Al_4Mn	$P6_3/m$	*hP*568	2.84	2.84	1.24	90	90	120	0.362	[21]
$Al_{13}Fe_4$	C2/m	*mS*102	1.55	0.80	1.25	90	107.7	90	0.371	[51]
Al_8Mn_5	R3m	*hR*26	1.27	1.27	0.79	90	90	120	0.355	[37]
LT-$Al_{11}Mn_4$	P-1	*aP*15	0.51	0.89	0.51	89.4	100.5	105.1	<0.1	[35]

of d-QC was in Mg-9Al-0.7Zn-0.06Mn (Al/Mn = 150) and the lowest in Mg-3Al-1Zn-0.5Mn (Al/Mn = 6).

The d-QC and (where present) LT-$Al_{11}Mn_4$ usually grew on the Al_8Mn_5 phase (e.g. Fig. 1(d)) which formed earlier in the solidification sequence, Fig. 1(a). Micrographs of typical microstructures of the Al-Mn IMCs at each combination of composition and cooling condition are given as Supplementary Information (Figure SI- 1). d-QC rods on the surfaces of Al_8Mn_5 were usually aligned in certain common directions as shown in Fig. 3(a)-(b), indicating an orientation relationship (OR) between the two phases. Typical TEM SAED results of the OR are shown in Fig. 3(c)-(f). Fig. 3(c)-(e) are SAED patterns along the d-QC d-2P direction, the Al_8Mn_5 $[0\bar{1}10]$ direction and a region containing both phases. Fig. 3(f) is the combination of the measured d-QC pattern (Fig. 3(c)) and the simulated Al_8Mn_5 pattern (simulated in the $[0\bar{1}10]$ direction of Fig. 3(d)) to help interpret the experimental pattern from both phases in Fig. 3(e). Note the overlapping spots along d-10 of the d-QC and $\{11\bar{2}0\}$ of Al_8Mn_5 in Fig. 3(f) which is associated with an excellent planar d-spacing match with ~0.16 % misfit. This OR can be expressed as Eq. (1) in the hexagonal setting and Eq. (2) in the body centred rhombohedral (BCR) setting of Al_8Mn_5:

$$\begin{aligned} &[\bar{2}110]_{Al8Mn5} // d-10 \\ &[0003]_{Al8Mn5} // d-2D \\ &[0\bar{1}10]_{Al8Mn5} // d-2P \end{aligned} \tag{1}$$

and

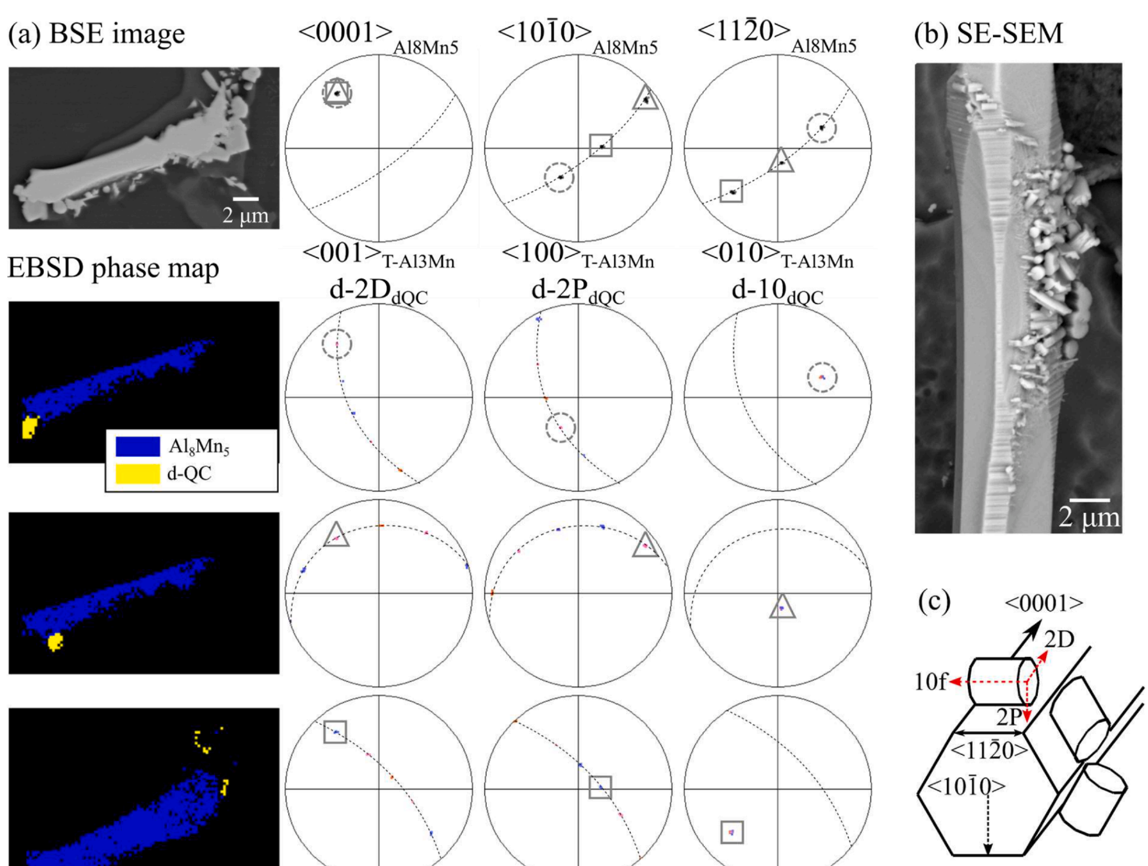

Fig. 4. EBSD analysis of the OR between Al_8Mn_5 and d-QC from AZ91–0.06Mn sample. (a) Cross-section through Al_8Mn_5 with multiple d-QC rods on its surface. Pole figures are shown for selected regions of d-QC highlighting one OR with three variants. The d-QC is indexed using the crystalline approximant T-Al_3Mn. (b) Multiple d-QC rods on Al_8Mn_5 after deep etching (c) schematic showing the d-QC on Al_8Mn_5 with the three variants of the OR.

$$\begin{matrix}[\bar{1}10]_{BCR}//d-10 \\ [111]_{BCR}//d-2D \\ [11\bar{2}]_{BCR}//d-2P\end{matrix} \quad (2)$$

Al_8Mn_5 is a rhombohedral gamma brass [24,36–38]. Previous studies have discussed gamma brasses as quasicrystal approximants [39,40,41,42], and, from structural considerations, the expected orientation relationship between cubic gamma brasses and d-QCs was predicted by Dong [39] to be: $[1\bar{1}0]$ // d-10; [001], [112] and [221] // d-2P; and [115], [111] and [110] // d-2D. Rhombohedral Al_8Mn_5 is related to the cubic gamma brasses by a small rhombohedral distortion ($\alpha \sim 89.1°$ when using a BCR unit cell) and small atomic shifts [36,37,24,38]. The OR measured here between Al_8Mn_5 and the d-QC is consistent with the OR predicted by Dong [39] for cubic gamma brasses when considering the reduction of symmetry to rhombohedral Al_8Mn_5.

The variants of the OR in Fig. 3 were studied by SEM EBSD. One approach to index quasicrystal EBSD patterns is to (mis)index them to a closely related crystalline approximant phase and then convert back to d-QC indices using the decagonal pseudosymmetry of the approximant [43,44]. To identify a suitable approximant for the Al-Mn-(Mg) d-QC, we compared experimental EBSD patterns from the d-QC with the range of d-QC approximants in Table 4 using Bruker DynamicS. The approach involved finding the dynamical simulated pattern of each approximant that best matched the measured d-QC EBSD pattern and then finding the closest matching approximant by comparing the cross-correlation coefficients. As shown in Table 4 the best match was to T-Al_3Mn (also known as HT-$Al_{11}Mn_4$) closely followed by R-Al_4Mn, (also known as π-Al_4Mn) and these were substantially better than the other candidate approximants. Consistent with this, both T-Al_3Mn [34,45,46], and R-Al_4Mn [14,47], are known to be approximants of the Al-Mn d-QC.

Past work [46] has shown that the Al-Mn d-QC and T-Al_3Mn are related by d-2P // $<100>_{Al3Mn}$, d-2D // $<001>_{Al3Mn}$ and d-10 // $<010>_{Al3Mn}$. In Fig. 4, the $<001>_{Al3Mn}$ pole figure contains five spots, each with a different colour, rotated 36° about <010> from the neighbouring spot, representing the ten d-2D directions (five in the northern hemisphere). The $<100>_{Al3Mn}$ pole figure also contains five spots, each rotated 36° about <010> from the neighbour, representing the ten d-2P directions, where each is rotated 18° about <010> from the nearest <001>. In the $<010>_{Al3Mn}$ pole figure, all five spots overlap in the d-10 direction. Considering the five pseudo-T-Al_3Mn orientations together gives the d-QC orientation.

In Fig. 4(a), multiple d-QC rods surrounded a single Al_8Mn_5 rod. There were three regions of d-QC rods and each region had the OR in Eq. (1) to the Al_8Mn_5 single crystal. The schematic in Fig. 4(c) highlights that the three variants arise because the d-10 axis of the d-QC can be parallel to any one of the three $<11\bar{2}0>$ axes of the Al_8Mn_5 rod, with a d-2D axis parallel to the $<0001>_{Al8Mn5}$ and a d-2P axis parallel to the $<10\bar{1}0>_{Al8Mn5}$ in each case. Examining the SE image of a deep etched Al_8Mn_5 rod in Fig. 4(b), notice that the d-QC rods mostly have one of three alignments relative to the Al_8Mn_5 rod, associated with the three variants of the OR.

During solidification, both the d-QC and LT-$Al_{11}Mn_4$ mostly grew on Al_8Mn_5 (e.g. Fig. 1(d)), the fraction of LT-$Al_{11}Mn_4$ decreased as the cooling rate increased (Table 4), and μ-Al_4Mn was not detected (Table 4). Thus, it is probable that the d-QC formed during solidification because it outcompeted the LT-$Al_{11}Mn_4$ (and possibly μ-Al_4Mn) phase(s) in terms of nucleation and/or growth on Al_8Mn_5. Note that, while the d-QC is best approximated by the T-Al_3Mn phase (Table 4), it also shares similar icosahedral building blocks with the LT-$Al_{11}Mn_4$ [35] and μ-Al_4Mn [33,52], phases and so the d-QC phase is outcompeting phases with which it shares structural similarities. We have previously reported ORs for LT-$Al_{11}Mn_4$ growing on Al_8Mn_5 during solidification at low cooling rate [10]. Those LT-$Al_{11}Mn_4$/Al_8Mn_5 ORs were more complex than the d-QC/Al_8Mn_5 OR found here and, often, the measured planes in the LT-$Al_{11}Mn_4$/Al_8Mn_5 OR were only nearly parallel [10]. From the simple and highly reproducible OR between the d-QC and Al_8Mn_5 in Fig. 3 and Fig. 4, it is likely that there is easier nucleation kinetics for the d-QC on Al_8Mn_5 than for LT-$Al_{11}Mn_4$ on Al_8Mn_5, which ultimately seems to arise from the structural relationship between quasicrystals and gamma brasses [39].

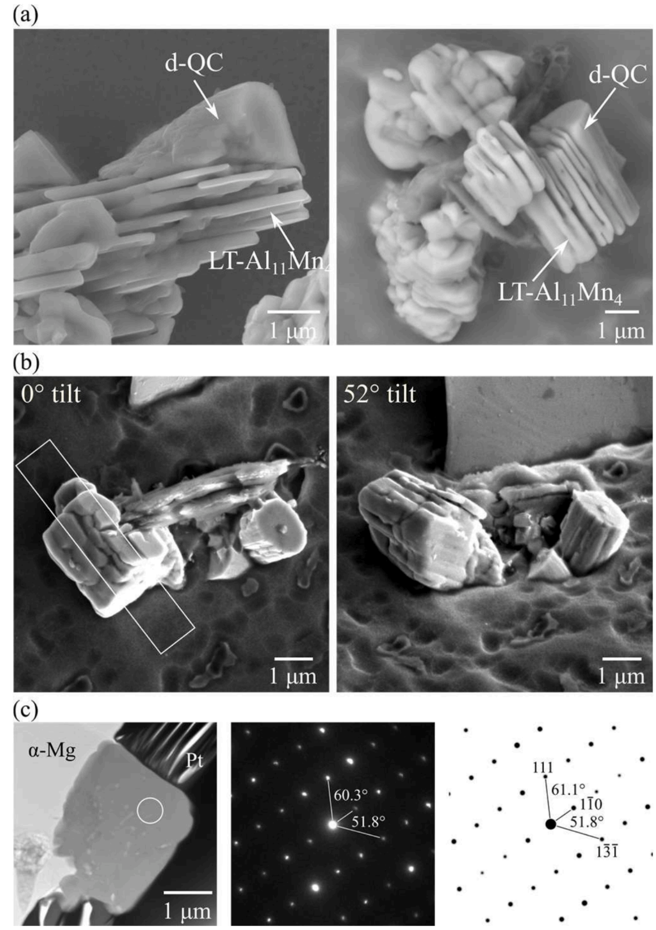

Fig. 5. Solid-state transformation of d-QC to LT-$Al_{11}Mn_4$ at 410 °C. (a) d-QC rods partially transformed to layers of LT-$Al_{11}Mn_4$ from the AZ91–0.06Mn sample held at 410 °C for 1 day and 15 days respectively; (b) SEM image of such a transformed rod in (a) from the AZ91–0.06Mn sample held at 410 °C for 15 days. A TEM lamella was lifted out by FIB in the white rectangle region. (c) ADF-STEM of the FIB lamellae in (b) and experimental and simulated SAED from the white circle region, viewed along LT-$Al_{11}Mn_4$ $[11\bar{2}]$. N.B. LT-$Al_{11}Mn_4$ = triclinic P-1 [35].

AZ91 alloys are often given a solution heat treatment of 16–24 h at 413 ± 6 °C [53] to dissolve the $Mg_{17}Al_{12}$ phase. Microstructures of the d-QC particles after 1 day and 15 days at 410 °C are shown in Fig. 5(a). The d-QC rods are in the process of transforming into parallel plates of LT-$Al_{11}Mn_4$, with a morphology similar to past work when Al_8Mn_5 transforms into LT-$Al_{11}Mn_4$ at 410 °C [10]. FIB lift-out and TEM analysis of a plate from a partially transformed d-QC rod is overviewed in Fig. 5 (b)-(c). The SAED pattern in Fig. 5(c) is along the $[11\bar{2}]$ zone axis of LT-$Al_{11}Mn_4$ and corresponding TEM EDS data are shown in Table 3. This transformation from d-QC to LT-$Al_{11}Mn_4$ shows that the d-QC is metastable at 410 °C.

In a similar AZ91 alloy, Zeng et al. [54] reported a decagonal Al-Mn-(Mg) phase of 20–200 nm size and Al:Mn ratio of 6.5 within the α-Mg phase, that was stable during solution treatment at 420 °C for 72 h. There are significant differences between the d-QC reported in that study [54] and the present paper. Here, the Al-Mn-(Mg) d-QC was ~2 μm, had an Al:Mn ratio of ~4.0, grew in the liquid in the latter stages of solidification, was usually attached to Al_8Mn_5, and was unstable at 410 °C where it transformed into LT-$Al_{11}Mn_4$. Therefore, further work is required to study Mn-bearing IMCs within the α-Mg matrix in AZ91 and understand how they relate to the d-QC that formed by solidification on Al_8Mn_5 in the present work.

In summary, an Al-Mn-based decagonal quasicrystal with composition $Al_{76.2}Mn_{20.2}Mg_{3.4}Fe_{0.2}$ (at.%) has been found in AZ-series alloys solidified at cooling rates from 0.1 K s^{-1} - ~90 K s^{-1}. It is an Al-Mn-type d-QC with periodicity around 12.3 Å. The d-QC was commonly found on the surfaces of Al_8Mn_5 with an OR involving three variants linked to the similarities between gamma brasses and quasicrystals. The d-QC formed in the latter stages of solidification where it outcompeted the equilibrium LT-$Al_{11}Mn_4$ phase (and possibly the μ-Al_4Mn phase) due to favourable nucleation on Al_8Mn_5 that forms earlier in the solidification sequence. The d-QC is a metastable phase at the typical solution heat treatment temperature of 410 °C where it transformed into LT-$Al_{11}Mn_4$.

Declaration of Competing Interest

The authors declare that they have no known competing financial interests or personal relationships that could have appeared to influence the work reported in this paper.

Acknowledgments

The authors gratefully acknowledge the use of characterisation facilities within the Harvey Flower Electron Microscopy Suite, Department of Materials, Imperial College London. This work was partially funded by the UK EPSRC Future LiME Hub (EP/N007638/1)

Supplementary materials

Supplementary material associated with this article can be found, in the online version, at doi:10.1016/j.scriptamat.2023.115886.

References

[1] A.S.T.M. International, Standard practice for codification of unalloyed magnesium and magnesium- alloys, cast and wrought, ASTM B951 (2018).
[2] E.F. Emley, “Principles of magnesium technology,” 1966.
[3] J.D. Hanawalt, C.E. Nelson, J.A. Peloubet, Corrosion studies of magnesium and its alloys, trans. AIME 147 (1942) 273–299.
[4] “TCMG4 database, Thermo-Calc 2019a.” 2019.
[5] X. Liu, et al., Heat-induced structural changes in magnesium alloys AZ91 and AZ31 investigated by in situ synchrotron high-energy X-ray diffraction, J. Mater. Sci. 57 (46) (2022) 21446–21459.
[6] J. Zhang, L. Pei, H. Du, W. Liang, C. Xu, B. Lu, Effect of Mg-based spherical quasicrystals on microstructure and mechanical properties of AZ91 alloys, J. Alloys Compd. 453 (1–2) (2008) 309–315.
[7] V.A.L.Y. Gertsman, J. Li, S.U. Xu, J.P. Thomson, M. Sahoo, Microstructure and second-phase particles in low- and high-pressure die-cast magnesium alloy AM50, Metall. Mater. Trans. A 36 (8) (2005) 1989–1997.
[8] G. Han, X. Liu, Phase control and formation mechanism of Al–Mn(–Fe) intermetallic particles in Mg–Al-based alloys with FeCl3 addition or melt superheating, Acta Mater 114 (2016) 54–66.
[9] G. Zeng, J.W. Xian, C.M. Gourlay, Nucleation and growth crystallography of Al8Mn5 on B2-Al(Mn,Fe) in AZ91 magnesium alloys, Acta Mater 153 (2018) 364–376.
[10] J.W. Xian, L. Peng, G. Zeng, D. Wang, C.M. Gourlay, Al11Mn4 formation on Al8Mn5 during the solidification and heat treatment of AZ-series magnesium alloys, Materialia 19 (2021), 101192. July.
[11] R. Sarvesha, et al., A study on the phase transformation of γ2-Al8Mn5 to LT-Al11Mn4 during solutionizing in AZ91 alloy, J. Alloys Compd. 873 (2021), 159836.
[12] Y. Wang, M. Xia, Z. Fan, X. Zhou, G.E. Thompson, The effect of Al8Mn5 intermetallic particles on grain size of as-cast Mg-Al-Zn AZ91D alloy, Intermetallics 18 (8) (2010) 1683–1689.
[13] J.L. Murray, A.J. McAlister, R.J. Schaefer, L.A. Bendersky, F.S. Biancaniello, D. L. Moffat, Stable and metastable phase equilibria in the AI-Mn system, Metall. Trans. A, Phys. Metall. Mater. Sci. 18 A (3) (1987) 385–392.
[14] S. Balanetskyy, G. Meisterernst, M. Heggen, M. Feuerbacher, Reinvestigation of the Al-Mn-Pd alloy system in the vicinity of the T- and R-phases, Intermetallics 16 (1) (2008) 71–87.
[15] B. Grushko, D. Pavlyuchkov, S.B. Mi, S. Balanetskyy, Ternary phases forming adjacent to Al3Mn-Al4Mn in Al-Mn-TM (TM = Fe, Co, Ni, Cu, Zn, Pd), J. Alloys Compd. 677 (2016) 148–162.
[16] K. Stan-Głowińska, Formation of quasicrystalline phases and their close approximants in cast Al-Mn base alloys modified by transition metals, Crystals 8 (2) (2018).
[17] D. Shechtman, I. Blech, D. Gratias, J.W. Cahn, Metallic phase with long-range orientational order and no translational symmetry, Phys. Rev. Lett. 53 (20) (1984) 1951–1953.
[18] L. Bendersky, Quasicrystal with one-dimensional translational symmetry and a tenfold rotation axis, Phys. Rev. Lett. 55 (14) (1985) 1461–1463.
[19] K. Chattopadhyay, S. Ranganathan, G.N Subbanna, N Thangaraj, Electron microscopy of quasi-crystals in rapidly solidified Al-14% Mn alloys, Scr. Mater. 19 (1985) 767–771.
[20] C.B. Shoemaker, D.A. Keszler, D.P. Shoemaker, Structure of μ-MnAl4 with composition close to that of quasicrystal phases, Acta Crystallogr. Sect. B 45 (1) (1989) 13–20.
[21] G. Kreiner, H.F. Franzen, The crystal structure of λ-Al4Mn, J. Alloys Compd. 261 (1–2) (1997) 83–104.
[22] J.J. Hu, P.L. Ryder, A new crystalline approximant of the decagonal phase in Al-Mn alloys, Philos. Mag. B Phys. Condens. Matter; Stat. Mech. Electron. Opt. Magn. Prop. 69 (4) (1994) 671–682.
[23] M.A. Taylor, Intermetallic phases in the Aluminium-Manganese binary system, Acta Metall 8 (4) (1960) 256–262.
[24] S. Thimmaiah, Z. Tener, T.N. Lamichhane, P.C. Canfield, G.J. Miller, Crystal structure, homogeneity range and electronic structure of rhombohedral γ-Mn5Al8, Zeitschrift fur Krist. - Cryst. Mater. 232 (7–9) (2017) 601–610.
[25] Y. Du, et al., Reassessment of the Al-Mn system and a thermodynamic description of the Al-Mg-Mn system, Zeitschrift fuer Met. Res. Adv. Tech. 98 (9) (2007) 855–871.
[26] S. Balanetskyy, D. Pavlyuchkov, T. Velikanova, B. Grushko, The Al-rich region of the Al-Fe-Mn alloy system, J. Alloys Compd. 619 (2015) 211–220.
[27] W. Zheng, et al., Thermodynamic investigation of the Al-Fe-Mn system over the whole composition and wide temperature ranges, J. Alloys Compd. 742 (2018) 1046–1057.
[28] C.J. Lin, L. Peng, J.W. Xian, Q. Li, C.M. Gourlay, Eutectic solidification in Mg-9Al-0.7Zn: from divorced to coupled growth, J. Alloys Compd. 938 (2023).
[29] K.K. Fung, C.Y. Yang, Y.Q. Zhou, J.G. Zhao, W.S. Zhan, B.G. Shen, Icosahedrally related decagonal quasicrystal in rapidly cooled Al-14-at.%-Fe alloy, Phys. Rev. Lett. 56 (19) (1986) 2060–2063.
[30] P.C. Gibbons, K.F. Kelton, S. Ranganathan, T.L. Daulton, Kikuchi bands in qnasicrystals and their approximants, Philos. Mag. A Phys. Condens. Matter, Struct. Defects Mech. Prop. 80 (4) (2000) 843–852.
[31] B. Grushko, T.Y. Velikanova, Stable and metastable quasicrystals in Al-based alloy systems with transition metals, J. Alloys Compd. 367 (1–2) (2004) 58–63.
[32] N.C. Shi, X.Z. Li, Z.S. Ma, K.H. Kuo, Crystalline phases related to a decagonal quasicrystal. I. A single-crystal X-ray diffraction study of the orthorhombic Al3Mn phase, Acta Crystallogr. Sect. B 50 (1) (1994) 22–30.
[33] C.B. Shoemaker, On the relationship between μ-MnAl4·12and the decagonal Mn-Al phase, Philos. Mag. B Phys. Condens. Matter; Stat. Mech. Electron. Opt. Magn. Prop. 67 (6) (1993) 869–881.
[34] J.D. Fitz Gerald, R.L. Withers, A.M. Stewart, A. Calka, The Al-Mn decagonal phase: 1. a re-evaluation of some diffraction effects: 2. relationship to crystalline phases, Philos. Mag. B Phys. Condens. Matter; Stat. Mech. Electron. Opt. Magn. Prop. 58 (1) (1988) 15–33.
[35] A. Kontio, E.D. Stevens, P. Coppens, R.D. Brown, A.E. Dwight, J.M. Williams, New investigation of the structure of Mn4Al11, Acta Crystallogr. Sect. B Struct. Crystallogr. Cryst. Chem. 36 (2) (1980) 435–436.
[36] K. Yoshida, T. Yamamoto, S. Nagata, Microstructure in MnAl (r) Alloy Phase, Jpn. J. Appl. Phys. 13 (3) (1974) 400–410.
[37] M. Ellner, The structure of the high-temperature phase MnAl (h) and the displacive transformation from MnAl (h) into Mn5AI8, Metall. Trans. A 21 (6) (1989) 19–22.
[38] Q. Hu, B. Wen, C. Fan, The structure of the aluminium-abundant γ-brass-type Al8.6Mn4.4, IUCrData 6 (9) (2021) 1–9.
[39] C. Dong, The δ-Al4 Cu9 phase as an approximant of quasicrystals, Philos. Mag. A Phys. Condens. Matter, Struct. Defects Mech. Prop. 73 (6) (1996) 1519–1528.
[40] S. Ranganathan, A. Subramaniam, A.P. Tsai, C. Dong, BCC derivative structures and their relation to rational approximants to quasicrystals, Ferroelectrics 250 (1) (2001) 201–206.
[41] V. Demange, J. Ghanbaja, F. Machizaud, J.M. Dubois, About γ-brass phases in the Al-Cr-Fe system and their relationships to quasicrystals and approximants, Philos. Mag. 85 (12) (2005) 1261–1272.
[42] S.P. Ge, K.H. Kuo, Ordered γ-brass structures coexisting with the decagonal quasicrystal in a Ga46Fe23Cu23Si8 alloy, J. Mater. Res. 14 (7) (1999) 2799–2805.
[43] G. Cios, et al., Approximant-based orientation determination of quasicrystals using electron backscatter diffraction, Ultramicroscopy 218 (2020), 113093. April.
[44] S. Singh, W.C. Lenthe, M. De Graef, Many-beam dynamical scattering simulations for scanning and transmission electron microscopy modalities for 2D and 3D quasicrystals, Philos. Mag. 99 (14) (2019) 1732–1750.
[45] T.L. Daulton, K.F. Kelton, P.C. Gibbons, Decagonal and related phases in Al-Mn alloys: electron diffraction and microstructure, Philos. Mag. B Phys. Condens. Matter; Stat. Mech. Electron. Opt. Magn. Prop. 63 (3) (1991) 687–714.
[46] K. Hiraga, M. Kaneko, Y. Matsuo, S. Hashimoto, The structure of Al3Mn: close relationship to decagonal quasicrystals, Philos. Mag. B Phys. Condens. Matter; Stat. Mech. Electron. Opt. Magn. Prop. 67 (2) (1993) 193–205.
[47] X.Z. Li, K.H. Kuo, The structural model of Al-Mn decagonal quasicrystal based on a new Al-Mn approximant, Philos. Mag. B 65 (3) (1992) 525–533.
[48] V.V. Pavlyuk, et al., Structure Refinement of Orthorhombic MnAl3, Acta Crystallogr. Sect. C Cryst. Struct. Commun. 51 (5) (1995) 792–794.

[49] K. Robinson, The determination of the crystal structure of Ni4Mn11Al60, Acta Crystallogr 7 (6) (1954) 494–497.
[50] Y. Matsuo, K. Hiraga, The structure of Al3Pd: close relationship to decagonal quasicrystals, Philos. Mag. Lett. 70 (3) (1994) 155–161.
[51] J. Grin, U. Burkhardt, M. Ellner, K. Peters, Refinement of the Fe4Al13 structure and its relationship to the quasihomological homeotypical structures, Zeitschrift fur Krist. - New Cryst. Struct. 209 (6) (1994) 479–487.
[52] L. Bendersky, Al-Mn μ phase and its relation to quasicrystals, J. Microsc. 146 (3) (1987) 303–312.
[53] ASTM International, "ASTM-B661-12. Standard practice for heat treatment of magnesium alloys," 2020.
[54] R. Zeng, Y. Chiu, I.P. Jones, Characterisation of nano-sized Al-Mn-(Mg) particles in AZ91 and their effect on Mg17Al12 precipitation, J. Alloys Compd. 579 (2013) 34–38.